communications biology

Article

https://doi.org/10.1038/s42003-024-07234-x

Saikogenin A improves ethanol-induced liver injury by targeting SIRT1 to modulate lipid metabolism

Mingzhu Jiang[1,2,4], Ying Feng[1,4], Jingxian Wang[1,4], Xiang Xu[1], Zegan Liu[2], Tongfei Li[1], Shinan Ma[1], Yufeng Wang[3] ✉, Xingrong Guo[1] ✉ & Shiming Du[1,2] ✉

Chronic alcohol consumption can lead to alcohol live disease (ALD). Steatosis is a critical hallmark of ALD, making it an important stage for therapeutic intervention. Saikosaponin A (SSa), a compound found in *Radix Bupleuri*, has previously shown promising hepatoprotective, anti-inflammatory, and antioxidant properties. However, its role in ALD remains understudied. We employ cell-based screening models and a chronic-plus-binge ethanol-fed mouse model to investigate the protective mechanisms of SSa and its metabolite Saikogenin A (SGA), against ethanol-induced hepatocyte injury. Our RNA-seq analysis in mice unveils that SSa primarily acts through the mTOR and PPAR-α signaling pathways in the liver. Biophysical assays and loss of function experiments confirm SGA directly binds to and modulates the activity of SIRT1 protein, mitigating ethanol-induced cell injury via the SIRT1-mTOR-PPAR-α axis. Furthermore, SGA displays a survival prolonging advantage compared to resveratrol for treating ALD. This suggests SGA holds promise as a potential therapeutic agent for ALD.

Excessive ethanol consumption stands as a prominent instigator of chronic live ailments on a global scale. The spectrum of alcoholic liver diseases (ALD) encompasses a variety of conditions, spanning from simple steatosis, and alcoholic steatohepatitis to alcoholic cirrhosis. ALD, afflicting more than million individuals globally, persists as a formidable public health challenge[1,2]. Nevertheless, effective, targeted therapies for ALD remain notably scarce. Typically, glucocorticoids, either used alone or in combination with pentoxifylline, is usually used in the clinical management of ALD. Regrettably, recent findings from the Steroid or Pentoxifylline for Alcoholic Hepatitis (STOPAH) trial further underscore the limitations efficacy of this regimen[3]. Furthermore, it has been recognized that years of steatosis can serve as an early predictor of the overall severity of the disease, which challenges the previous notion that steatosis is a benign condition[4]. Notably, steatosis caused by alcohol consumption is the main factor of ALD. Hence, early intervention for the alcohol-induced steatosis may hold the key to impeding the progression of ALD to more advanced stages.

Radix Bupleuri, is a kind of traditional Chinese medicine, has garnered widespread recognition for its effectiveness in treating diverse liver diseases[5]. Saikosaponin a (SSa) is a pivotal saikosaponin within *Radix bupleuri*, which has a triterpenoid glycoside structure strikingly reminiscent of steroid hormones[6,7]. Contemporary advancements in phytochemistry and biomedical research have unveiled SSa's diverse therapeutic attributes, including hepatoprotective properties[8], anti-inflammatory capabilities[9], antioxidant potential[10], immunoregulatory functions[11], and even anticancer properties[12]. Our previous study showed that SSa can improve alcoholic-induced liver injury by regulating lipid metabolism, suggesting that SSa may have a therapeutic effect on alcoholic-induced steatosis.

Saikosaponins has been shown to have poor oral availability. When exposed to gastric acid, the SSa hydrolyzes to Saikosaponin B1 (SSB1), a compound containing isocyclodiene. Under the action of gut microbiota, SSB1 is hydrolyzed by β-D-glycosidase and ultimately transformed into Saikogenin A (SGA). Through the above metabolic transformation, the final product SGA has a stronger absorption and utilization rate[13–15]. We meticulously assessed the plasma concentrations of SSa, SSB1, and SGA after oral administration of SSa by ultra-high-performance liquid-chromatography-MS/MS (UHPLC-MS/MS). We found that SSA and SSB1 were quickly metabolized after administration, while SGA

[1]Hubei Key Laboratory of Embryonic Stem Cell Research, Hubei Provincial Clinical Research Center for Umbilical Cord Blood Hematopoietic Stem Cells, Department of neurosurgery, Taihe Hospital, School of Pharmaceutical Sciences, Hubei University of Medicine, Shiyan, China. [2]Hubei Key Laboratory of Wudang Local Chinese Medicine Research, Taihe Hospital, Hubei University of Medicine, Shiyan, China. [3]Institute for Systems Genetics, New York University, New York, NY, USA. [4]These authors contributed equally: Mingzhu Jiang, Ying Feng, Jingxian Wang. ✉e-mail: yufeng.wang@nyulangone.org; gxrdl@hbmu.edu.cn; dushiming@taihehospital.com

remained stable and persistent. Elucidating whether SSa, SSB1 or SGA improves alcoholic-induced steatosis will help guide clinical trials and applications.

Sirtuin 1 (SIRT1), a member of the nicotinamide adenine dinucleotide-dependent class III protein deacetylases[16], has been shown to play an important role in regulating hepatic metabolism and physiology. SIRT1 is also recognized as a sensor of cellular nutrient that controls lipid homeostasis in liver. In young mouse, liver overexpression of SIRT1 alleviates obesity-induced endoplasmic reticulum (ER) stress and insulin resistance[17]. Moreover, the deficiency of SIRT1 in hepatocytes exacerbates the progression of ALD by promoting liver steatosis, inflammation and ER stress; conversely, overexpression of SIRT1 alleviates high-fat-diet-induced hepatic steatosis. The abnormal expression of SIRT1 induced by alcohol consumption is associated with lipid accumulation, inflammation, and hepatocyte necrosis. Therefore, pharmacologic and genetic activation of SIRT1 could effectively reverse the ALD progression. As one of the activators of SIRT1, resveratrol has been shown to be effective in the treatment of ALD[18,19]. These previous studies indicated that SIRT1 has emerged as a promising therapeutic target for ALD[20,21]. Thus, given the significant antioxidant and hepatoprotective effects of SSa, we sought to investigate its therapeutic potential in an ALD murine model and whether its therapeutic potential involves targeting SIRT1 if any.

Results

SSa effectively improved alcohol-induced liver injury in chronic-plus-binge ethanol-fed mice

As previously described, based on that a proportion of ALD patients also carry a history of chronic drinking accompanied by acute excessive alcohol consumption. A chronic-plus-binge alcohol-feeding mice model was employed in our study[22,23], the detailed modeling and grouping information of mice is shown in Fig. 1A. There was no significant difference in food intake among all mice in this study (Supplementary Fig. S1A). Comparing with the control mice, ethanol feeding significantly reduced body weight and increased liver index, while SSa treatment improved body weight and liver index in a dose-dependent manner (Fig. 1B, C). Compared to the livers of control mice, the appearance of the livers of mice in the alcohol-fed group was light yellow and greasy, whereas SSa treatment significantly changes the alcohol-induced liver appearance(Supplementary Fig. S1B). HE staining was used to evaluate the pathological changes of liver tissue. The livers of alcohol-fed mice exhibited typical histological abnormalities, including macrophage infiltration, hydropic degeneration and lipo-droplet vacuole, and SSa treatment improves liver pathological injury (Fig. 1D and Supplementary Fig. S1C). Lipid deposition in liver was further analyzed by Oil red O staining. The liver lipid deposition of alcohol-fed mice was significantly higher than that of the control group, and SSa treatment reduced alcohol-induced liver lipid deposition in a dose-dependent manner (Fig. 1E and Supplementary Fig. S1D). Consistent with the liver pathology described above, SSa treatment significantly ameliorated liver function and reduced the plasma TC, TG, γ-GT content and De Ritis ratio under alcohol feeding (Fig. 1F and Supplementary Fig. S1E). The TC, TG, and NAD^+/NADH content in liver homogenate were also detected, and the results showed that SSa significantly reduced alcohol-induced TC and TG accumulation in the liver, but increased the NAD^+/NADH ratio (Fig. 1G and Supplementary Fig. S1F), which indicated that SSa may improve liver function and lipid metabolism in ALD mice.

In order to evaluate the short-term toxicity of SSa, male C57BL/6J mice (aged 8 weeks) were treated with SSa (15 mg/kg/daily) for 14 consecutive days by gavage. The pathological changes of liver, kidney, spleen, lung and heart was analyzed by HE staining. And the results suggested that there were no significant pathological changes in the above organs (Supplementary Fig. S1G). These findings demonstrated that SSa alleviates alcohol-induced liver injury in a dose-dependent manner, and SSa has no obvious toxicity to the body.

Transcriptome and metabolomics analysis shows that SSa regulates hepatic lipid metabolism

To elucidate the mechanism of SSa in improving alcohol-induced liver injury, the RNA-Seq and metabolomics analysis of the liver tissue from alcohol-fed and alcohol-fed combined with high-dosage SSa mice (Fig. 2A). Differentially expressed genes and metabolites were showed by volcano maps, and the Kyoto Encyclopedia of Genes and Genomes (KEGG) pathway enrichment were conducted according to these differentially expressed genes and metabolites (Fig. 2B, C). According to the KEGG analysis, the PPAR-α and mTOR signaling pathways were significantly different. It has been reported that PPAR-α and mTOR signaling pathways play an important role in ALD by regulating fatty acid oxidation and adipogenesis[24–26]. Therefore, we speculate that SSa may protect form alcohol-induced liver injury through PPAR-α and mTOR pathways. DEP domain-containing mTOR-interacting protein (Deptor) limits the activity of mTOR kinase by binding to mTOR[27]. Additionally, cleaved caspase-3 expression was limited in the livers of SSa-treated ALD mice[28]. We then detected the expression of lipid metabolity-related genes such as p-mTOR, PPAR-α, Deptor and PGC-1α, and the results showed that alcohol promotes the phosphorylation of mTOR and the shear of caspase-3 and decreases the expression of PPAR-α, PGC1-1α and Deptor, while the SSa treatment could reverse these phenomena in a dose-dependent manner (Fig. 2D and Supplementary Fig. S2A).

As one of the important downstream of the mTOR pathway, SREBP-1C plays a role in various pathophysiological processes by regulating lipid metabolism[29]. We also Real-time PCR analysis analyzed the mRNA expression of SREBP-1C and its downstream target gene such as acetyl-CoA carboxylase (ACC-1), fatty acid synthase (FAS), and stearoyl CoA desaturase 1 (SCD-1) in the liver tissue (Fig. 2E). As shown in Fig. 2F, SSa treatment decreased the elevation of SREBP-1C, ACC-1, FAS and SCD-1 induced by alcohol. Based on the previous sequencing results, we did a Protein-Protein Interaction Networks analysis and found that the PPAR-α and mTOR signaling pathways were linked tightly through the central molecule called SIRT1 (Fig. 2G). SIRT1 has been reported to ameliorate ALD by regulating hepatic lipid metabolism, limiting hepatic inflammation and modulating hepatic fibrosis. We analyzed the GEO database and found that the expression of SIRT1 in the liver of ALD patients including alcoholic steatosis, mild acute alcoholic and alcohol hepatitis was significantly decreased than that in the normal population (Fig. 2H). Furthermore, our findings also demonstrated that alcohol challenge decrease the expression of SIRT1 in the liver, and SSa treatment can reverse this phenomenon (Fig. 2I, J and Supplementary Fig. S2B). As a transcription factor, SIRT1 plays a role mainly by entering the nucleus to regulate the expression of downstream target genes (Please see Fig. 8 in refs. 30–33). In our study, mice liver were stimulated by alcohol and SSa. Immunofluorescence results showed that alcohol reduced SIRT1 entry into the nucleus, while SSa treatment promoted SIRT1 entry into the nucleus (Fig. 2K and Supplementary Fig. S2C). These findings suggests that SSa regulates liver lipid metabolism mediated by PPAR-α and mTOR signaling pathways by activating SIRT1, thereby improving alcohol-induced liver injury.

SSa metabolite SGA reduces ethanol-induced cell damage by activating SIRT1 in vitro

Although we have demonstrated that SSa improves alcohol-induced liver damage, studies have demonstrated that the poor absorbance in the intestine when administered orally and toxicity induced by marked hemolysis under intravenous injection limited the application of SSa[34,35]. It has been reported that SSa can be metabolized into SSB1 and SGA by gastrointestinal tract (Fig. 3A). Our study also assessed the content of SSa, SSB1, and SGA in plasma at various time points over the course of 24 h after intragastric administration of SSa (50 mg/kg). Initially, a standard system that can simultaneously detect SSa, SSB1, and SGA was constructed on a liquid chromatography-tandem mass spectrometer and the characteristic peaks of three drugs (Supplementary Fig. S3A). The blood concentration analysis indicated that the maximal plasma concentration of SSa was attained 30 min

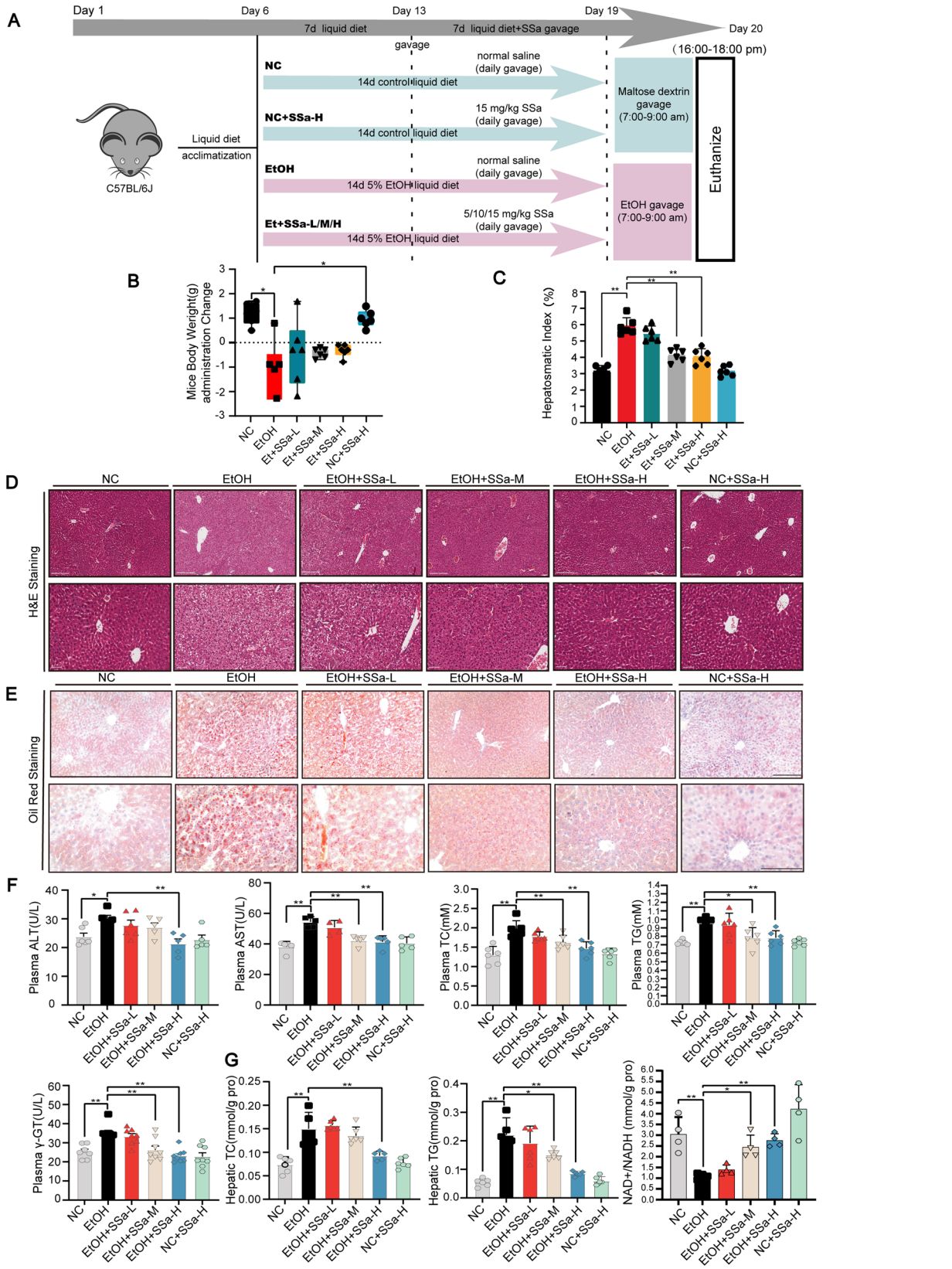

Fig. 1 | SSa effectively limited liver injury in chronic-plus-binge ethanol-fed mice. **A** Schematic representation of the experiment, and timeline of administration of SSa solution. **B** SSa influenced the reduced body weight of mice administered with ethanol from day 12 to day 19 ($n = 6$ per group). Data are represented as the mean ± SD, $^{*}p < 0.05$, $^{**}p < 0.01$ between the two groups. **C** The levels of liver/body weight index ($n = 6$). **D**, **E** representative liver H&E staining (Bar:200 and 60 μm) and Oil Red O staining images from mice with ALD and/or SSa cotreatment (Scale Bar: 100 and 75 μm) ($n = 3$). **F** Differences in plasma biochemical parameters (ALT, AST, TC, TG, and γ-GT) in mice cotreated with ALD and/or SSa ($n = 6$). **G** Alterations in hepatic parameters (TC, TG, and NAD^{+}/NADH) in mice with ALD and/or SSa cotreatment ($n = 6$).

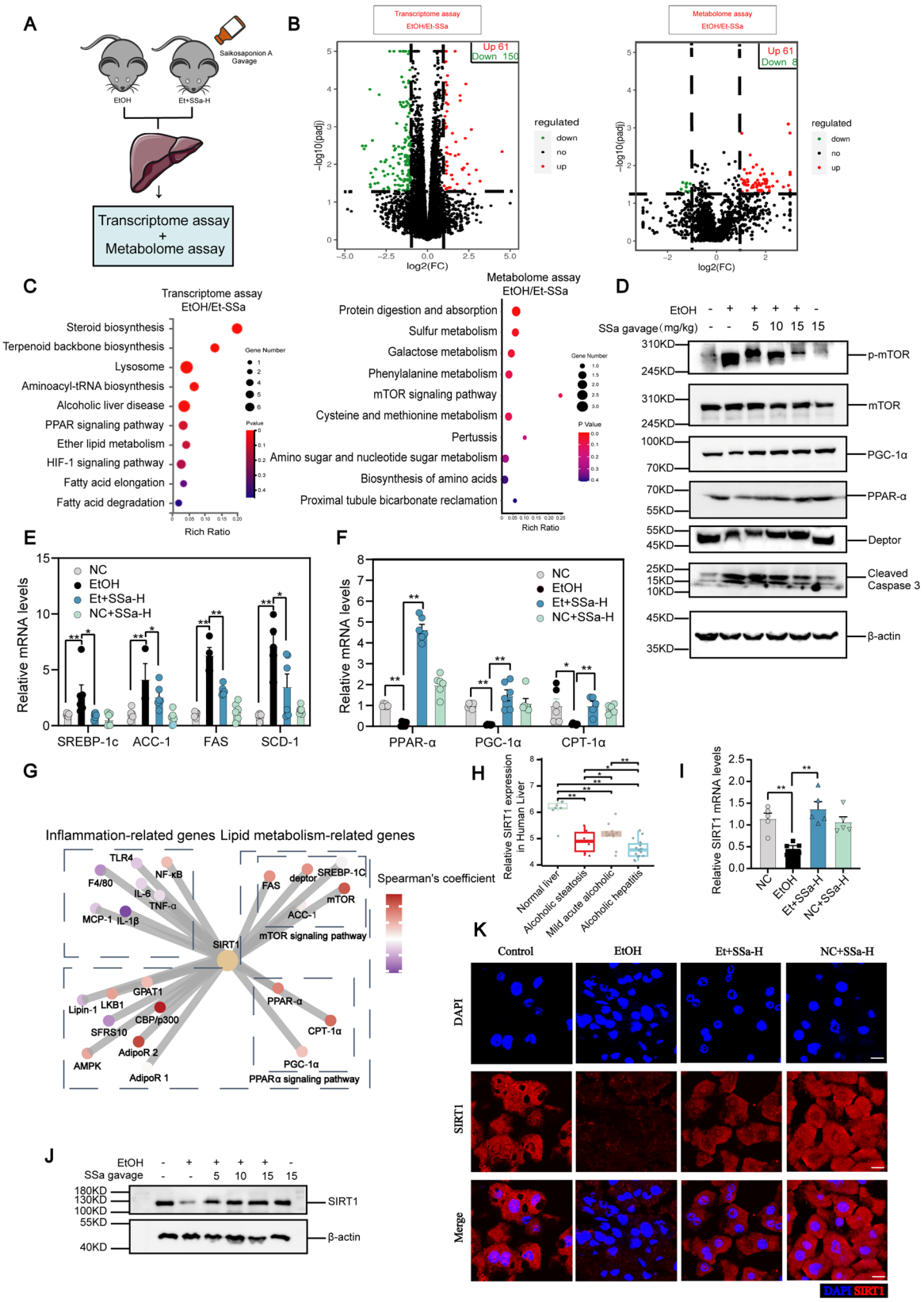

after administration (63.31 ng/mL). The SSB1 was detected 0.5 h after administration, and the peak concentration was 105.12 ng/mL 1 h after administration. SSa was almost completely metabolized after 2 h of administration, while SSB1 was undetectable after 6 h of administration. However, the SGA, as a metabolic product of SSa, was not detected till at 2 h after administration, and its levels increased steadily over a 2–8 h period. The highest SGA content was 66.31 ng/mL at 8 h after administration (Fig. 3B). Additionally, between 0 and 12 h, SSa enhanced hepatic SIRT1 protein abundance at 4–12 h (Fig. 3C and Supplementary Fig. S3B). To further examine the effects of SSa, SSB1, and SGA on ethanol-induced

Fig. 2 | Multiomics uncovers that oral SSa solution modulated hepatic lipid profile. A Scheme of RNA-seq assays and metabolite analysis strategies employing the EtOH and Et+SSa-H group mouse livers ($n = 4$ in each group). **B** Volcano plot results of differentially expressed genes and metabolites in the Et+SSa-H vs. EtOH groups. **C** Kyoto Encyclopedia of Genes and Genomes pathway enrichment analysis of the identified differentially expressed genes and metabolites according to RNA-seq and metabolite data sets from the Et+SSa-H vs. EtOH groups. **D** Protein level alterations in phosphorylated mTOR, total mTOR, PGC- 1α, PPAR-α, Deptor, and cleaved caspase-3 in the liver from mice containing ALD and/or SSa cotreatment ($n = 3$). **E**, **F** mRNA abundance of SREBP- 1C and PPAR-α possessing their target genes in the liver from mice with ALD and/or SSa cotreatment ($n = 6$). Data are represented as the mean ± SD, $^{*}p < 0.05$, $^{**}p < 0.01$ between the two groups. **G** Correlation of SIRT1 expression with the expression profiles of genes linked to lipid metabolism in mouse livers according to RNA-seq data. **H** Combination of GSE28619 and GSE103580 data with batch effect examination of SIRT1 expression. **I** mRNA abundance of SIRT1 in the liver from mice with ALD and/or SSa cotreatment ($n = 6$). **J** Protein level alterations of SIRT1 in the liver from mice with ALD and/or SSa cotreatment ($n = 3$). **K** Representative confocal microscopy images (Scale Bar: 20 μm) of immunostaining targeting SIRT1 in mouse liver ($n = 3$).

cellular damage, we stimulated HepG2 cells with ethanol or comnined with SSa, SSB1 and SGA, respectively. The Oil red O staining analysis showed that SSa and SGA significantly reduced the lipid droplet accumulation induced by ethanol while SSB1 had no significant effect (Fig. 3D, E). We found that ethanol can also increase the production of ROS, and SSa and SGA treatment significantly limited ethanol-induced ROS production, while SSB1 had no effect on ROS (Fig. 3F, G). These results showed that SSa and SGA can improve ethanol-induced cell damage, but SSB1 had no effect.

The occurrence of blood SGA was found to be consistent with the activation of SIRT1, we examined the regulatory effect of SGA on SIRT1 expression. Both RT-PCR and Western blot analyses indicated that SGA reversed the inhibition of SIRT1 expression in HepG2 cells caused by ethanol (Fig. 3H, I and Supplementary Fig. S4C, D). The PPAR-α inhibitor GW6471 and the mTOR activator MHY1485 were used to analyze whether SGA improved ethanol-induced lipid deposition and ROS production in HepG2 cells depending on PPAR-α and mTOR signal pathways. The results showed that inhibition of PPAR-α or mTOR abolishes the protection of SGA against ethanol-induced cellular peroxidative damage and lipid droplet deposition in HepG2 cells (Fig. 3J–M and Supplementary Fig. S4E–I). These findings demonstrate that SSa metabolites SGA ameliorates ethanol-induced cellular damage by regulating SIRT1 mediated PPAR-α and mTOR signaling pathways.

SGA reduces ethanol-induced cell damage by directivity binding to SIRT1

SIRT1 is a principal target for the treatment of ALD[36]. To clarify the mechanism of SIRT1 activation of SGA, we assessed the interactions between the SIRT1 kinase domain and SGA via molecular docking. The results indicated that the hydrogen bonds were formed between SGA GLY-415, GLU-416, and GLN-345 residues of SIRT1, respectively. And the hydrophobic interactions between SGA and PHE-414, PHE-297, PHE-273, VAL-412, and HIS-363 of SIRT1 were also found (Fig. 4A and Supplementary Table 1). Microscale thermophoresis (MST) assays were conducted to quantify the binding affinity between SGA and SIRT1. And the results showed that the Kd between SIRT1 and SGA is ~23.764 μM, and the Kd between SIRT1 and SSa and SSB1 is ~25.176 μM and 97.617 μM, respectively (Fig. 4B), which indicated that the binding ability of SGA with SIRT1 is stronger than SSa and SSB1. We compared the effects of SSa and SGA on the viability of human normal LO2 cells (Fig. 4C), and determined that SGA had a higher median normalized IC50 than SSa (SGA:79.83 μmol/L; SSa:11.05 μmol/L). This demonstrated that the conversion of SSa to SGA by hydrolysis in vivo had an increased safety profile for hepatocytes. In order to confirm that SGA improve ethanol-induced cellular damage by activing of SIRT1, the small interfering RNA (siRNA) was used to silence the expression of SIRT1 in HepG2 cells. Flow cytometry and Oil red O staining analyses indicated that SIRT1 silencing blocks the protection of SGA against cellular peroxidative damage and elimination of cellular lipid droplet deposition induced by ethanol (Fig. 4D–G). Western blot analysis demonstrated that SIRT1 silencing decreases SGA-induced increased PGC-1α, Deptor and PPAR-α expression and increases the SGA-induced suppressing of p-mTOR under alcohol stimulation (Fig. 4H and Supplementary Fig. S4A). Collectively, these data suggest that SGA ameliorated ethanol-induced cellular damage likely by directivity binding to SIRT1, and then activating PPAR-α and suppressing mTOR activity. In primary hepatocytes cells we also found that that SGA enhanced SIRT1 expression and induced SIRT1 expression in the nucleus, also SGA could activator SIRT1 expression with physiological condition in primary hepatocytes cells. (Fig. 4I and Supplementary Fig. S4B).

SSa improves alcohol-induced liver damage dependent on SIRT1 in vivo

To further clarify SSa treatment of alcohol-induced liver injury by activating SIRT1, we knocked down SIRT1 expression in hepatocytes using AAV8-packaged shRNA (Fig. 5A–C). The food intake of mice in each group was similar, SIRT1 knockdown had no effect on body weight of mice after continuous SSa administration for 7 days (Fig. 5D and Supplementary Fig. S5A). The knockdown of SIRT1 had no effect on the normal mice liver function, but mitigated SSa's improvement in alcohol-induced liver function recovery (Fig. 5E). Our results also suggested that the absence of SIRT1 attenuates the improvement in the liver morphology induced by SSa treatment (Supplementary Fig. S5B). The HE staining and Oil red O staining suggested that the deficiency of SIRT1 prevents the SSa's improvement in alcohol-induced hepatic pathology and lipid deposition (Fig. 5F, G and Supplementary Fig. S5C, D). Although SIRT1 deficiency had no obvious effect in TC and TG contents in plasma and liver homogenate, SIRT1 deficiency hindered the improvement of alcohol-induced liver function, plasma TC and TG contents and the TC, TG and γ-GT content of liver homogenate by SSa treatment (Fig. 5H, I and Supplementary Fig. S5E). Moreover, in the absence of SIRT1, the increase of NAD^{+}/NADH induced by SSa was also inhibited (Fig. 5H, I and Supplementary Fig. S5F). These data suggested that SIRT1 deficiency has no influence on liver function and lipid metabolism and SSa treatment improves alcohol-induced liver injury by activating SIRT1.

SSa induced expression of SIRT1 improve alcohol-induced liver injury by PPAR-α and mTOR signal pathway

To determine whether SSa-induced expression of SIRT1 improves alcohol-induced liver injury through the PPAR-α and mTOR pathway, we examined the expression of downstream genes. The Western blot results suggested that the SIRT1 deficiency decreases the expression of PGC-1α, PPAR-α and Deptor induced by SSa treatment. Moreover, SIRT1 deficiency also increased the phosphorylation of mTOR, which was decreased during SSa treatment (Fig. 6A and Supplementary Fig. S6). Real-time PCR analysis was used to assess the mRNA expression of lipid metabolism genes related to PPAR-α and mTOR pathway, and the results showed that SIRT1 knockdown inhibits the upregulation of PGC-1α, PPAR-α, CPT-1α induced by SSa on the transcription level after alcohol stimulation (Fig. 6B). Furthermore, SSa treatment decreased the mRNA expression of SREBP-1C, ACC1, FAS and SCD-1, while SIRT1 knockdown reversed these phenomenons (Fig. 6C). Immunofluorescence analysis also demonstrated that alcohol increases the expression of SREBP-1C and SIRT1 deficient upregulates SREBP-1C expression which can be inhibited by SSa treatment (Fig. 6D, E). These results demonstrated in vivo that SIRT1 deficiency can abolish the regulation of SSa on PPAR-α and mTOR signaling pathways, which suggested that SSa treatment improve alcohol-induced live injurey through SIRT1 mediated PPAR-α and mTOR signaling pathways.

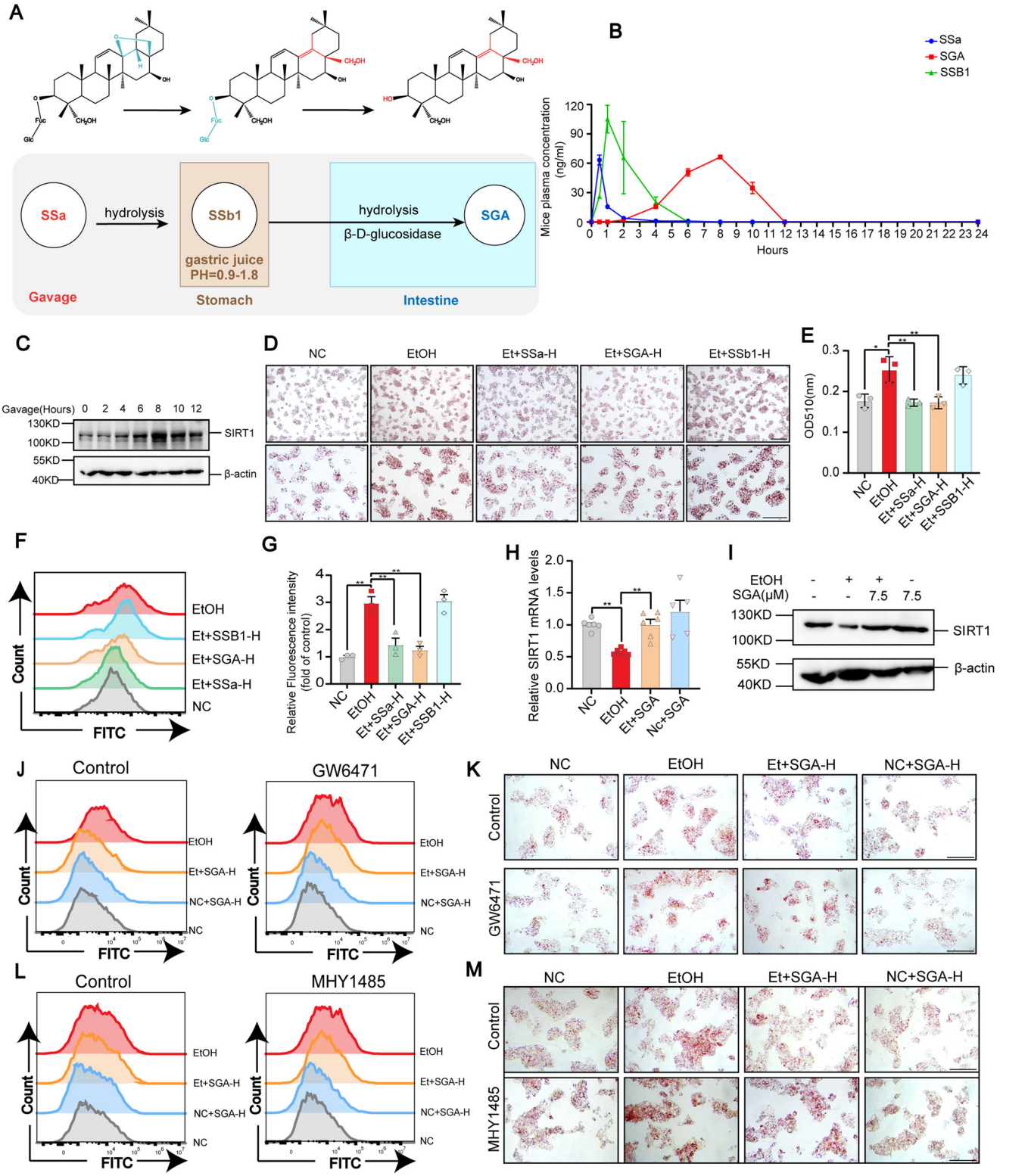

Fig. 3 | SGA promotes SIRT1 activity and limits ethanol-induced cell damage in vitro. A The disposition pathways of Saikosaponin a to Saikogenin a in mice following oral administration. **B** Plasma concentration-time courses of Saikosaponin a and its metabolites in mice after oral SSa solution (50 mg/kg) administration ($n = 3$). **C** Protein level changes in hepatic SIRT1 over time after gavage with SSa solution ($n = 3$). **D**, **E** Effects of Saikosaponin a and its metabolites (7.5 μmol/L) on ethanol-induced lipid storage in HepG2 cells as detected by Oil Red O staining (Scale Bar:100 and 75 μm), The cell samples were eluted using isopropanol and the optical density (OD) of the solution at 510 nm was measured. **F**, **G** After administration of Saikosaponin a and its metabolites to ethanol-treated cells, the ROS levels were examined by flow cytometry (FCM) in HepG2 cells ($n = 3$). **H** mRNA abundance of SIRT1 with ethanol and/or SGA treatment in HepG2 cells ($n = 6$). **I** Protein level alterations in SIRT1 with ethanol and/or SGA treatment in HepG2 cells ($n = 3$). **J**, **K** ROS levels were analyzed by FCM with ethanol and/or SGA (7.5 μmol/L) cotreatment, with or without GW6471/MHY1485 treatment in HepG2 cells (Scale Bar:75 μm) ($n = 3$). **L**, **M** Effects of SGA (7.5 μmol/L) on ethanol-induced lipid storage with or without GW6471/MHY1485 treatment in HepG2 cells as detected by Oil Red O staining (Scale Bar:75 μm) ($n = 3$).

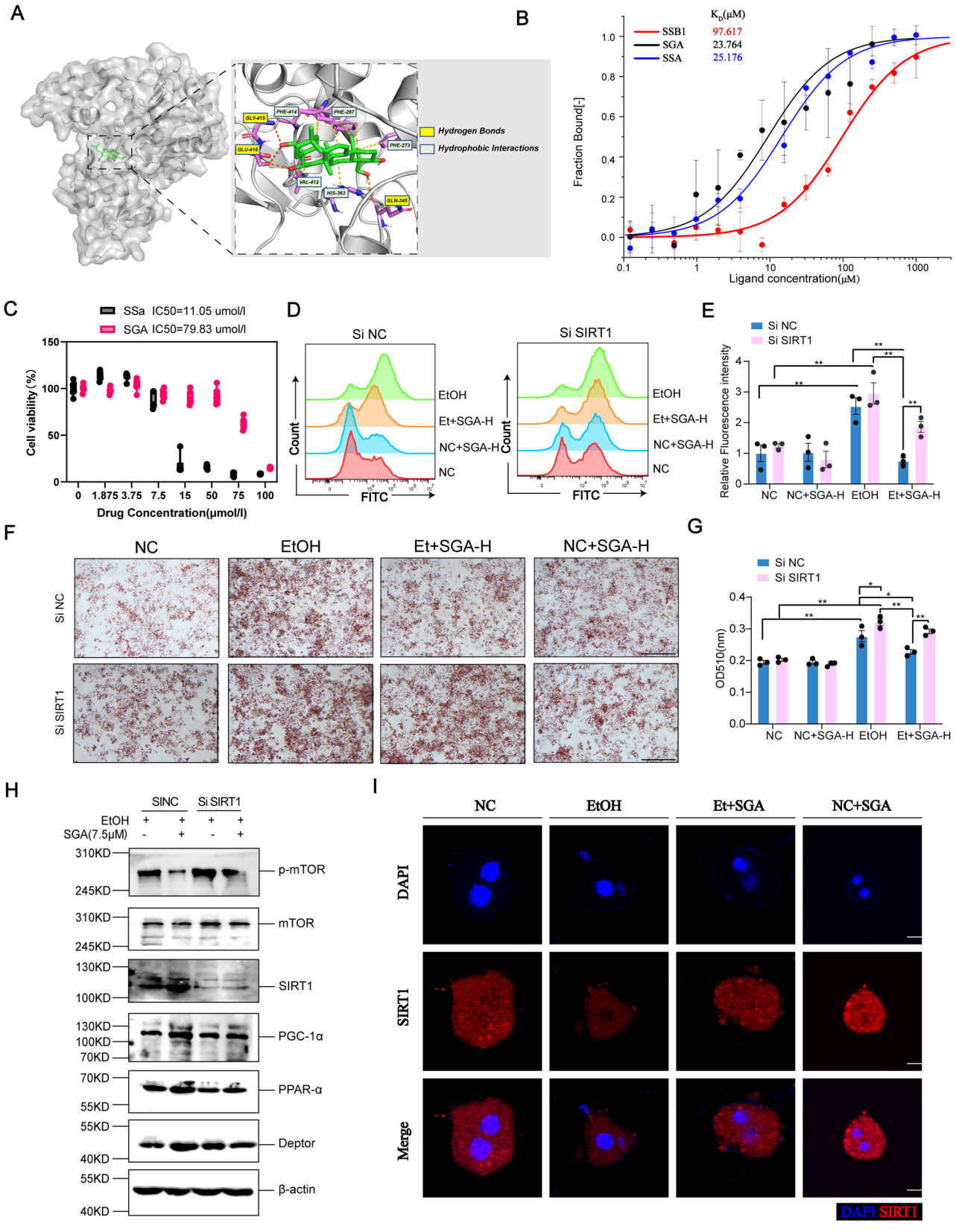

SGA ameliorates ethanol-induced liver injury

Previously, we found that SGA was safer for hepatocytes than the prototype drug and had good binding ability to human SIRT1 protein, and was able to ameliorate ethanol-induced hepatocyte injury in vitro in agreement with the prototype drug. We further explored the pharmacodynamic effects of SGA in vivo in ALD mice and compared it with resveratrol, a SIRT1 activator, which has been reported to have the same ameliorating effect on ALD. The drug doses were given according to the refs. 18,19,37,38 (Fig. 7A), Under the condition that food intake was similar across each group (Supplementary Fig. S7A) and the results showed that administration of all three drugs for

Fig. 4 | SGA binds SIRT1 and improves ethanol-induced cell damage likely via the SIRT1-PPAR-α/mTOR axis. A Molecular modeling analysis of SSa to the catalytic binding site of the SIRT1 kinase domain. Left: Complete view of SSa in the binding site of SIRT1 (cartoon). Right: close-up view of SSa in the binding sites of SIRT1 (surface). **B** Microscale thermophoretic analysis of SSa and its metabolites SSB1 and SGA and their interactions with SIRT1. The NHS-ester RED dye binds covalently to the Recombination Human SIRT1 protein lysine side chain and was incubated with increasing concentrations of SSa, SSB1, or SGA, and the binding reactions were subjected to MST. SSa, SSB1, and SGA bind to SIRT1 with Kd values of 25.176 μmol/L, 97.617 μmol/L, and 23.764 μmol/L, respectively. **C** Cells were subjected to various concentrations of SGA or SSa for 24 h. Logarithmic transformation of SGA or SSa concentrations and cell viability data were fitted to a nonlinear regression curve (log(inhibitor) vs. response-variable slope) to ascertain the LC50 of LO2 ($n = 6$). **D**, **E** FCM was employed to analyze the ROS levels with ethanol and/or SGA cotreatment, with or without SIRT1 knockdown in HepG2 cells ($n = 3$). **F**, **G** Oil Red O staining detected lipid droplets with ethanol and/or SGA cotreatment, with or without SIRT1 knockdown in HepG2 cells (Scale Bar:75 μm) ($n = 3$). **H** Protein level changes in phosphorylated mTOR, total mTOR, SIRT1, PGC- 1α, and PPAR-α with ethanol and/or SGA cotreatment, with or without SIRT1 knockdown in HepG2 cells ($n = 3$). **I** Representative confocal microscopy images (Scale Bar:20 μm) of immunostaining targeting SIRT1 in primary hepatocytes cells from mice ($n = 5$).

one week failed to reverse ethanol-induced body weight loss in mice (Fig. 7B), but all three drugs ameliorated ethanol-induced abnormalities of Liver/BW index (Fig. 7C). We also tested the hepatic effects of three drugs on ALD mice and found that all drugs ameliorated the inflammatory cell infiltration and lipid droplet accumulation induced by ethanol (Fig. 7E, F and Supplementary Fig. S7B–F). However, SGA administration could improve survival of ALD model mice compared with resveratrol administration (Fig. 7D).

Discussion

ALD is caused by excess alcohol intake and is life-threatening with little approved therapy[39]. Although some agents such as corticosteroids and pentoxifylline have been used[40,41], the largest human alcoholic hepatitis trial, the STOPAH trial, demonstrated their ineffectiveness. Recent insights suggest that the degree of lipid degeneration might play a pivotal role in the overall disease process, offering hope for novel therapeutic interventions for ALD management[42–44]. Increasing evidence has demonstrated the health-promoting properties of SSa in various liver disease models, such as lipopolysaccharide and d-galactosamine-induced liver injury[45], nonalcoholic fatty liver disease[46] and liver fibrosis[47]. Given the unique steroid-like structure and significant antioxidant and hepatoprotective effects of SSa, we sought to investigate its therapeutic potential in an ALD murine model.

In traditional Chinese medicine, *Radix Bupleuri* has a long history of use in preventing and treating various liver diseases[48]. SSa, one of its primary active components, has undiscovered treatment potential in ALD. Elucidating the receptor proteins targeted by SSa is highly valuable for elucidating the pharmacological mechanisms of Radix Bupleuri and expanding the clinical applications of SSa. Our findings indicated that oral administration of SSa solution efficiently mitigated lipid accumulation in this ALD animal model. Through high-throughput sequencing and molecular biology analyses, we revealed that SSa ameliorated ethanol-induced hepatic lipid accumulation by modulating the PPAR-α and mTOR signaling pathways. Furthermore, we investigated the pharmacological activity of the metabolites of SSa after oral administration and found that even if there is structural instability of SSa in gastric fluid, the pharmacodynamic efficacy of SSa does not rely solely on the original compound. This study is the first to evaluate the pharmacodynamic effects of SSa, its metabolite SSB1, and SGA on ALD.

To explore the mechanism by which SSa improves ALD, we used RNA-Seq and metabolomics to analyze the gene expression and metabolite expression profiles in the alcohol-fed and high-dosage SSa groups. Our findings indicated that SSa could restore the dysregulation of the PPAR-α and mTOR signaling pathways, which is linked to the increase in SIRT1 protein expression. The receptor SIRT1 is pivotal for controlling lipid metabolism, inflammation, and ALD development in the human liver[49,50]. One such receptor, SIRT1, is pivotal in controlling lipid metabolism, inflammation, and ALD development in the human liver. Bioinformatics analyses and biophysical studies have shed light on the robust binding capacity of both SSa and its metabolic end-product SGA to the SIRT1 protein. Notably, SGA and SSa activated hepatic SIRT1 protein expression under normal and ethanol-induced pathological conditions. Knocking down hepatic SIRT1 expression somewhat attenuated the efficacy of oral SSa solution in ALD mice, indicating that SSA ameliorated ALD through the dependent activation of SIRT1. SIRT1's role as a central mediator in the protection conferred by oral SSa in ALD. Nevertheless, the possibility of other receptors for SSa and its metabolites cannot be ruled out.

Bioinformatics and biophysical analyses revealed that SSa and its metabolite SGA strongly bind to the SIRT1 protein, and the ability of SGA to bind to SIRT1 protein is the strongest. Therefore, we speculate that SGA (the final metabolite of SSa in vivo) may directly interact with SIRT1 protein, thereby activating its activity and improving ALD. Our further results demonstrated that, compared with SSa, SGA has decreased toxicity in LO2 cells, and MST assays also showed an enhanced ability to bind to the SIRT1 protein in vitro. These findings indicated that SGA exerts pharmacodynamic effects by activating the SIRT1-PPAR-α/mTOR signaling pathway to improve liver injury in ALD mice.

SIRT1 reportedly modulates numerous activities by controlling gene expression, DNA repair, metabolism, the oxidative stress response, mitochondrial function, and biogenesis. In recent years, many studies have shown that SIRT1 is activated by several plant-based bioactive compounds, such as curcumin[51], catechins[52], Berberine[53], fisetin[54], and resveratrol[18,19], and many clinical trials have also been conducted on SIRT1 activators (NCT02114892, NCT03675724, NCT01732393, and NCT01925547). Some clinical trials suggest potential therapeutic effects of these SIRT1 modulators. Therefore, we compared the effects of SGA and resveratrol on ALD in vivo, and the results showed that SGA administration could improve survival of ALD model mice compared with resveratrol administration. Therefore, designing an SGA administration route is our goal in the future. Identifying suitable drug traces in vivo could facilitate the exploration of the binding between SGA and SIRT1. A change in the structure of SGA through hydrolytic transformation can aid in binding to the SIRT1 protein. Resolving the key motifs in the structure of SGA during its binding to the SIRT1 protein may assist in the design of small-molecule agonists of SIRT1 with enhanced pharmacological activity.

In conclusion, our data suggested that SGA ameliorated ethanol-induced cellular damage likely by binding to the SIRT1 protein, activating PPAR-α and suppressing mTOR activity. Thus, our study identified a new potential candidate to activate SIRT1 via a relatively defined mechanism of action. This advance may provide hope for ALD patients.

Methods

Chemicals and reagents

Saikosaponin A (SSa), Saikosaponin B1(SSB1), Saikogenin A (SGA) and Resveratrol (Res) were acquired from TargetMol (Boston, USA). An antibody (Ab) against SIRT1 was obtained from Abcam (Cambridge, USA). Abs targeting PPAR-α and PGC-1α were procured from MCE (Monmouth, USA). Abs against mTOR, phospho-mTOR, Deptor, Caspase-3, β-actin, and goat anti-rabbit IgG were purchased from ABclonal (Wuhan, China).

The antibodies used in the study are listed in Supplementary Table 2. Recombinant human SIRT1 protein was acquired from SinoBiological (Beijing, China). A Cell Counting Kit-8 was obtained from New Cell & Molecular Biotech (Suzhou, China). MHY1485 and GW6471 were procured from TargetMol (Boston, USA), while 2'7'-Dichlorofluorescin diacetate and Modified Oil Red O stain kits were obtained from Solarbio (Beijing, China). Alanine aminotransferase (ALT), Aspartate

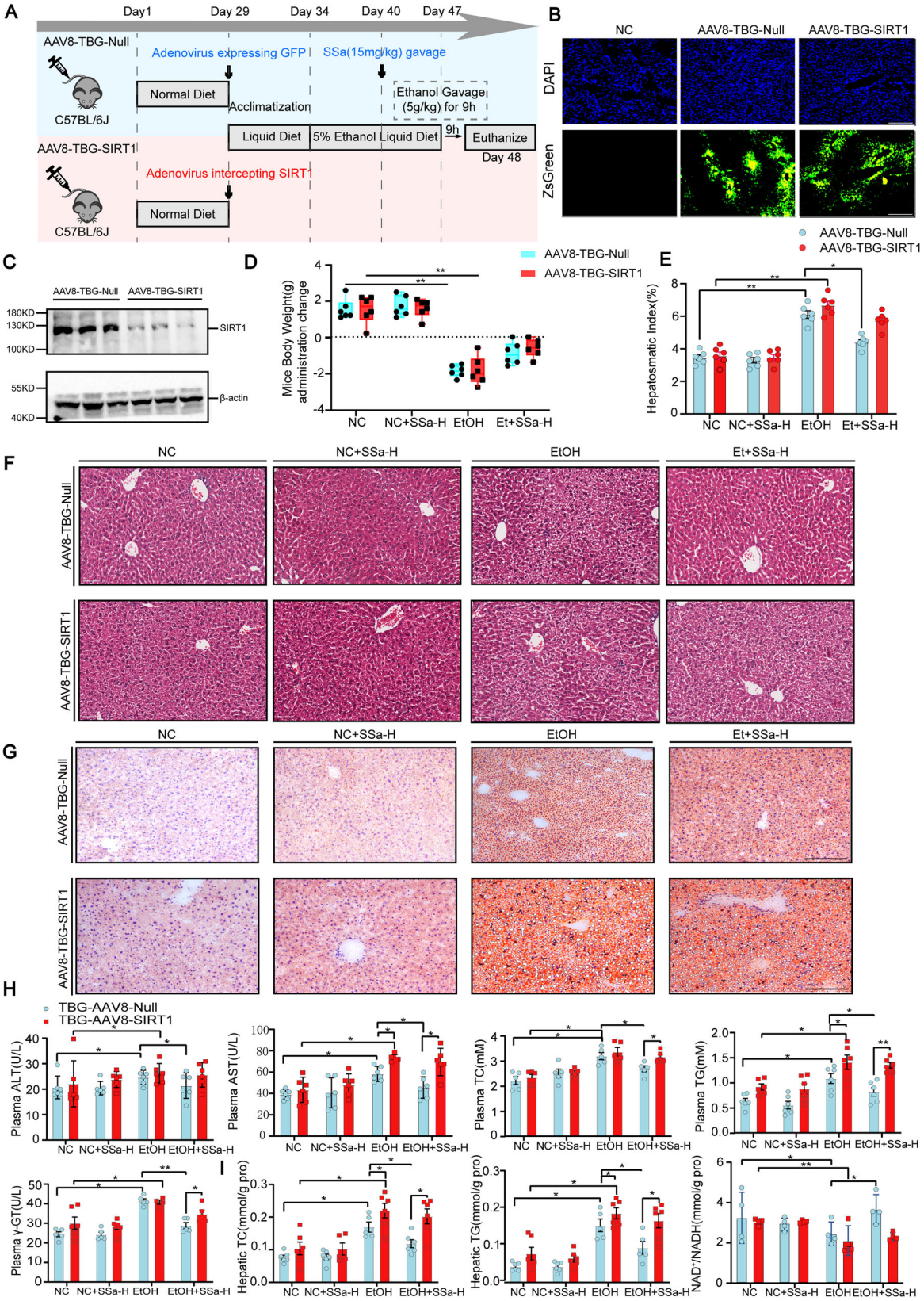

aminotransferase (AST), Triglyceride (TG), Total cholesterol (TC), γ-glutamyl transferase (γ-GT), Nicotinamide Adenine Diphosphate (NAD^+) and Nicotinamide Adenine Dinucleotide (NADH) commercial kits were all acquired from the Nanjing Jiancheng Bioengineering Institute (Nanjing, China).

Animal models and treatment

C57BL/6J male mice aged eight weeks old were acquired from the Center for Animal Experiments/Animal Biosafety-III Laboratory at the Hubei University of Medicine. All mice were maintained in temperature-controlled cages (23 to 25 °C) with precise humidity (50% ± 5%) under a 12-h light/12-

Fig. 5 | SIRT1 is associated with oral SSa solution-mediated alleviation of ethanol-induced liver damage. A Schematic knockdown of hepatic SIRT1 in C57BL/6J mice and a timeline of NIAAA mouse model construction. **B** Representative immunofluorescence microscopy images from liver cryosections (Day 28). Detection of fluorescence signaling of the AAV8 vector with ZsGreen fluorescent tag. **C** Alterations in hepatic SIRT1 protein levels were assessed in mice with or without hepatic SIRT1 knockdown (Day 50) ($n = 3$). **D** Alterations in body weight of mice given SSa with or without hepatic SIRT1 knockdown ($n = 6$). **E** The levels of liver/body weight index ($n = 6$). **F**, **G** Representative liver H&E (Scale Bar:60 μm) and Oil Red O staining images from mice with ALD and/or SSa cotreatment, with or without hepatic SIRT1 knockdown ($n = 3$). **H** Alterations in plasma biochemical parameters (ALT, AST, TC, TG, and γ-GT) in mice with ALD and/or SSa cotreatment, with or without hepatic SIRT1 knockdown ($n = 6$). **I** Changes in hepatic parameters (TC, TG, and NAD^+/NADH) in mice with ALD and/or SSa cotreatment, with or without hepatic SIRT1 knockdown ($n = 6$).

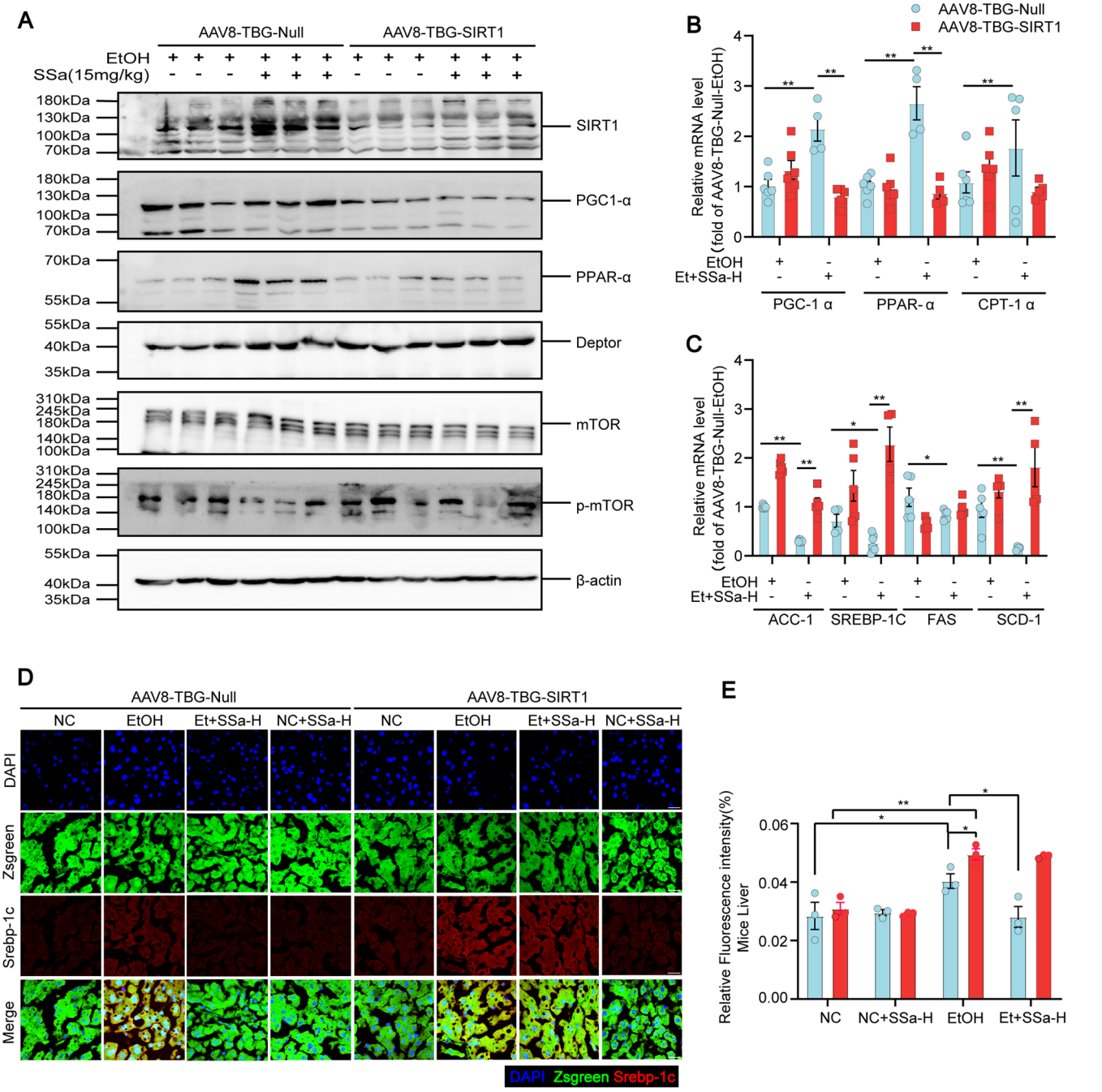

Fig. 6 | SIRT1-PPAR-α/mTOR transmits oral SSa solution-mediated protection signals in ALD mice. A Protein level alterations in total mTOR, phosphorylated mTOR SIRT1, PGC- 1α, PPAR-α, and Deptor with ALD and/or SGA cotreatment, with or without hepatic SIRT1 knockdown (Day 50) ($n = 3$). **B**, **C** mRNA abundance of hepatic SREBP- 1C, PPAR-α and their target genes with ALD and/or SSa treatment, with or without hepatic SIRT1 knockdown ($n = 6$). **D**, **E** Representative confocal microscopy images (Scale Bar:20 μm) of immunostaining of SREBP- 1C in mouse liver, and quantification of the SREBP- 1C positive area ($n = 3$).

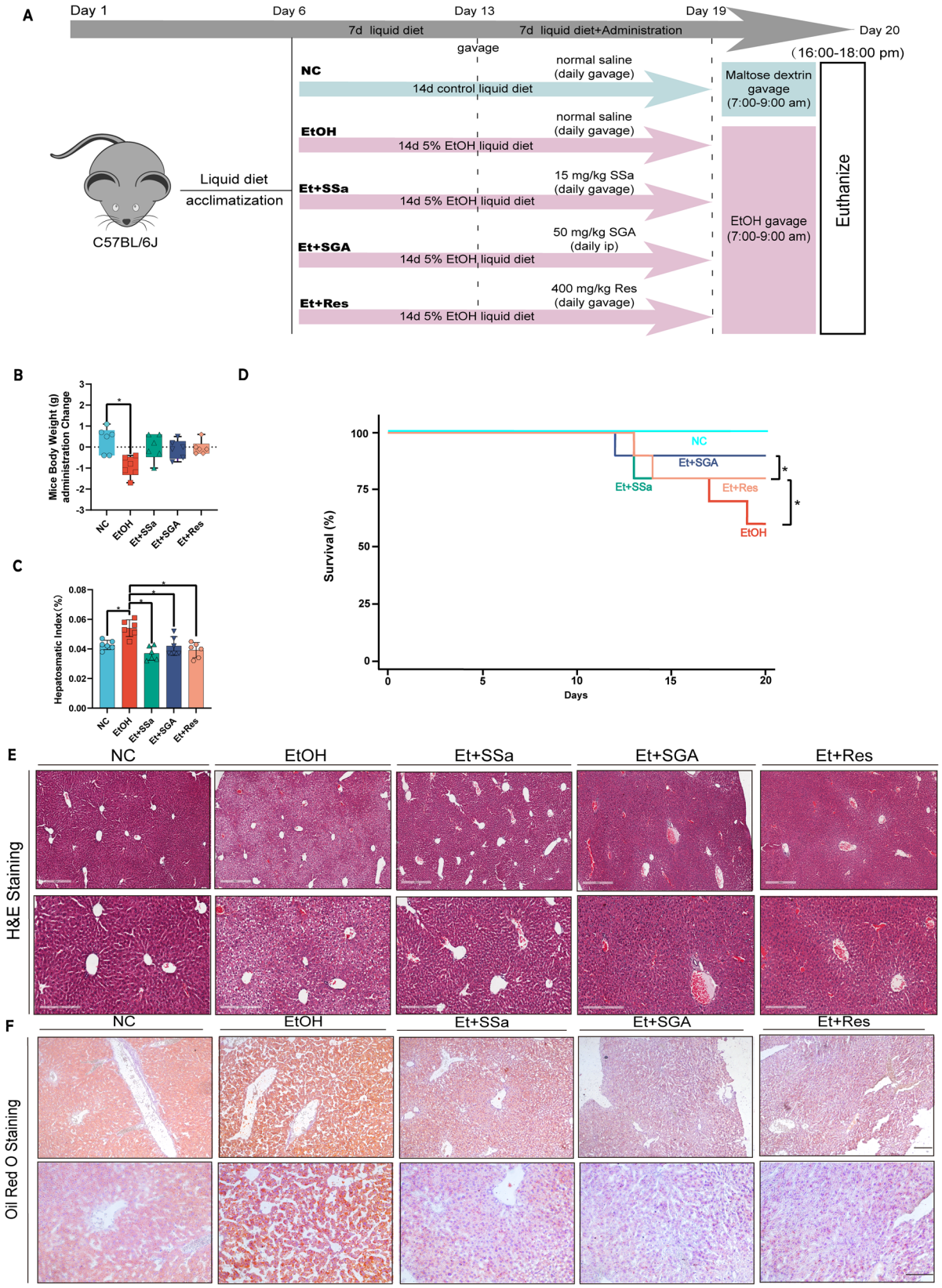

Fig. 7 | SGA ameliorates ethanol-induced liver injury. A Schematic representation of the experiment, and timeline of administration of SSa and SGA and Res. **B** SSa and SGA and Res influenced the reduced body weight of mice administered with ethanol from day 12 to day 19 ($n = 6$ per group). **C** The levels of liver/body weight index ($n = 6$). **D** Survival of the mice under treatment of the three drug, respectively. **E, F** Representative liver H&E staining (Bar: 200 and 60 μm) and Oil Red O staining images from mice with ALD and/or SSa cotreatment (Scale Bar: 100 and 75 μm) ($n = 3$).

h dark cycle. The mice were allowed access to sterilized food and water ad libitum. All animal assessments received the approval of the Experimental Animal Ethics Committee at the Hubei University of Medicine Animal Center. We have complied with all relevant ethical regulations for animal use.

Chronic-binge ethanol-fed mouse model

The mice underwent a one-week period of acclimatization to their surroundings prior to the commencement of the experiments. For the induction of alcoholic liver injury, the well-established animal model recommended by the National Institute on Alcohol Abuse and Alcoholism (NIAAA) was employed, with slight adjustments incorporated[22]. Specifically, following 5 days of acclimatization to the administration of a Lieber–DeCarli liquid control diet (Xietong Pharmaceutical Bioengineering Co. Ltd, Nanjing, China) ad libitum, the mice were randomly separated into six groups (8-12 per group). These groups encompassed an alcohol-fed (EtOH) group, alcohol-fed accompanied by oral SSa solution treatment (Et+SSa; 5,10, and 15 mg/kg) groups, a pair-fed (NC) group, and a pair-fed accompanied by oral SSa solution treatment (NC+SSa;15 mg/kg) group. The mice in the four EtOH groups received a Lieber–DeCarli ethanol (5% V/V) liquid diet for 14 days. On the 8th day, The NC and NC+SSa groups were administered a control diet consisting of isocaloric maltose dextrin. Mice within the SSa-treated groups were provided with SSa solution daily at 5, 10, or 15 mg/kg[46]. The SGA-treated groups with i.p. injection of SSa (50 mg/kg)[37,38]. The Res-treated groups were given 400 mg/kg Resveratrol by gavage[18,19], All of the medicines were to be taken Qd for 7 days. On the 15th day, all mice were given an oral dose of ethanol or isocaloric maltose dextrin. All mice were anesthetized with isoflurane after nine hours to harvest relevant samples.

Pharmacokinetic animal treatment

The mice were separated into ten groups with 9 mice in each group, consisting of pre-and post-administration subsets (Each sample contains a mixture of blood from three mice, $n = 3$ each). All mice were fasted 24 h prior to drug administration, which was provided as a 50 mg/kg dosage by oral gavage. Approximately 100 μL of blood was collected from the retro-orbital plexus from 9 animals per group at specific time points (0 h, 0.5 h, 1 h, 2 h, 4 h, 6 h, 8 h, 10 h, 12 h, and 24 h) following drug administration.

Construction of AAV8-TBG-shRNA and animal treatment

The vector genome was parceled into capsids derived from adeno-associated virus 8 (AAV8) through triple transfection of HEK293 cells. The vector genome contained a thyroxine-binding globulin (TBG) promoter. To improve the efficiency, the AAV mirR30-based shRNA knockdown vector system was employed for the knockdown of hepatic SIRT1 expression in vivo. The sequence of the shRNA employed was GCCATGTTTGATATTGAGTAT. These shRNAs were inserted into and AAV8-miR30 vector expressing the TBG promoter alongside ZsGreen. C57BL/6J mice were separated into two groups and injected with AAV8-TBG-miR30-1-m-SIRT1-ZsGreen and AAV8-TBG-ZsGreen (acquired from Hanheng Biotechnology, Shanghai, China) via the tail vein (at a dosage of 1×10^{12} vg/mouse). Four weeks after the injection, mice underwent NIAAA model establishment and drug administration.

Histological analysis

Liver tissues were initially subjected to fixation using 4% paraformaldehyde. The tissues were then embedded and thinly sliced (5 μm thick). Liver sections were visualized using hematoxylin and eosin (H&E) staining, Oil Red O staining, and immunofluorescence (IF) based on standard protocols[55,56]. H&E liver sections were scanned using an automatic digital slide scanner (Aperio CS2, Leica, Germany). ORO liver sections were assessed using a light microscope (DM2500, Leica, Germany). The IF liver sections were examined using confocal microscopy (FV3000RS, Olympus, Japan). Images were acquired digitally using an oil immersion lens at 100× objective magnification. The positive areas were examined using Image-Pro Plus software in 3 fields which were randomly selected in each sample.

RNA sequence analysis and data processing

The livers of mice in the EtOH and Et+SSa-H groups were sent to BGI (Shenzhen, China) for RNA sequencing. The RNA purity and concentration were measured using a Nanodrop spectrophotometer (Agilent 2100, USA). cDNA libraries were generated using the instructions provided by the manufacturer. The raw sequencing data were filtered using SOAPnuke (v.1.5.6) to acquire clean data, which was contrasted with the reference gene set utilizing Bowtie2 (v.2.3.4.3). Gene expression was determined using RSEM (v.1.3.1) software. Differential gene detection was conducted using DESeq2 (v.1.4.5), if the p-value was <0.05. All differentially expressed genes were employed for volcano plot generation and Kyoto Encyclopedia of Genes and Genomes (KEGG) ontology enrichment analyses.

Metabolomic examination and data processing

Metabolite extraction was conducted using the manufacturer's instructions (BGI, Shenzhen, China) as outlined previously[57]. A Waters 2777C Ultra Performance Liquid Chromatography (Waters, USA) alongside a Q Exactive HF high-resolution mass spectrometer (Thermo Fisher Scientific, USA) was utilized for metabolite separation and detection. The mass spectrometry data were imported into the Compound Discoverer 3.3 (Thermo Fisher Scientific, USA) program and integrated with the BMDB (BGI Metabolome Database), mzCloud database, and ChemSpider online database. Following analysis of the mass spectrometry data, a data matrix including data on metabolite peak areas and identification results was generated. The results were imported into mataX for data preprocessing. Identification of differentially abundant metabolites at a level of $p < 0.05$ using univariate analysis was conducted via volcano plots and KEGG enrichment analysis.

Pharmacokinetics analysis

Concentrations of 20 μg/L SSa, SSB1, and SGA stock solutions were mixed and diluted with mouse plasma to acquire QC and calibration standard samples. UHPLC-MS/MS (LC-TQ 5200 and LC 2000, Hexin Instrument Co. Ltd, Guangzhou, China) was employed to identify the blood concentration of the three drugs within mice. The calculation of the area under the concentration-time curve (AUC) involved employing moment analysis along with a logarithmic trapezoidal approach. Blood from three animals was obtained to detect the concentration of drugs at each time point, and was averaged for PK analysis. The Numerical Analysis Program for Pharmacokinetics (NAPP) was utilized for subsequent analyses.

Cell culture and transfection

HepG2 cells were acquired from the American Type Culture Collection (Manassas, VA, USA). Cells were grown in Dulbecco's modified Eagle's medium supplemented with 10% (V/V) fetal bovine serum at 37 °C along with 5% CO_2 in a maintained incubator. Cells were fasted for 12 h before the treatment. To induce ALD-like injury to HepG2 cells, they were treated with a concentration of 200 mmol/L ethanol for 24 h as previously reported[58,59]. Following this, cells were cotreated with various levels of drugs (1.875 to 5 μmol/L) as well as 200 mmol/L ethanol for 24 h. For RNA interference, the siRNA target sequences employed in this study were designed as follows: SIRT1 siRNA, 5′-GCCTGATGTTCCAGAGAGA-3′. siRNA was constructed by RiboBio (Guangzhou, China). HepG2 cells were transfected with SIRT1-siRNA or scramble siRNA for 18 h, and the cells were then incubated with 200 mmol/L ethanol for 24 h. MHY1485 and GW6471 were diluted to a concentration of 10 μmol/L[60,61] and the cells were incubated with both the drugs and ethanol for an additional 24 h.

Isolation of primary mouse liver cells

Primary mouse hepatocytes (PMHs) was isolated by in situ retrograde perfusion of the with IV type of collagenase digestion medium as reference described[62].

Molecular docking procedure

We employed human SIRT1 data acquired from the Protein Data Bank (PDB) database (PDB code:4ZZI) for our modeling[63]. The SGA structure was converted to MOL2format using the Open Babel GUI. Ligands and water molecules were excluded to generate 4ZZI (Ligand:4TQ 1NS Zn). Molecular docking was conducted using 4ZZI with SGA using AutoDock Tools (1.5.7) with a grid box center at (X:5.6, Y:37.2, Z: −2.4) blind docking was used. The grid box was employed to wrap the entire protein grid box (92 × 126 × 126 Å points). To characterize the optimal binding sites, the count of independent docking iterations conducted for each simulation was established at 50 with 2,500,000 energy assessments in each iteration. We used the docking conformation possessing the lowest binding energy in PyMol to visualize the protein-ligand docking orientation[64].

Microscale thermophoresis

Recombinant human SIRT1 protein was labeled using a Monolith RED-NHS Protein Labeling Kit (MO-L011, Nanotemper Technologies, Munich, Germany). Specifically, 90 μL of protein was combined with 10 μL of marker dye and incubated for 30 min at room temperature in darkness, before being filtered through a gel column. A pre-test step was conducted to examine the protein labeling efficiency, protein adsorption, and aggregation phenomena prior to beginning the experiment. Protein dilutions (in a volume of 10 μL) were incubated with 10 μL of SSa/SSB1/SGA (with a maximum concentration of 1 mmol/L, which was double-diluted into 16 different concentrations) diluted in MST RNA buffer (consisting of 20 mmol/L HEPES-HCL pH 8.0, 0.1 mol/L NaCl, 20 mmol/L $MgCl_2$, 1 mmol/L DTT, and 0.1% (V/V) Tween-20) for 5 min at 24 °C. Thermophoresis and temperature jump data were baseline-corrected and employed to calculate Kd using NanoTemper analysis software (MO affinity analysis V.2.3.) and plotted with Origin Pro 2018.

Quantitative real-time polymerase chain reaction (qRT-PCR)

Total RNA was isolated from liver tissues or HepG2 cells using RNAiso (Takara, Kyoto, Japan). Synthesis of cDNA was conducted using a Superscript Kit for RT-PCR (Lablead, Beijing, China). qRT-PCR was performed with a reaction volume of 10 μL containing 25 nmol/L forward and reverse primers, alongside a 1×SYBR Green reaction mix (QIAGEN, Netherlands, Germany) and a concentration of 3.5 nmol/L template. Detailed primer information can be found in the Supplementary Table 3. β-Actin was employed as a reference control, and data analysis was carried out using the delta-delta Ct method. Five biological replicates were conducted for the qPCR experiments.

Western blot

Liver tissues or HepG2 cells were the source of total protein extraction, and its quantification was determined using the BCA reagent provided by Bio-Rad. A total of 20 μg of the extracted protein was loaded and subjected to separation using 10% SDS-PAGE. The separated proteins were subsequently transferred onto PVDF membranes, followed by a one-hour blocking step with 5% skim milk. Post-blocking, the membranes were exposed to the designed primary antibodies overnight at a temperature of 4 °C. After undergoing three washes with TBST, the membranes were then treated with a horseradish peroxidase-conjugated secondary antibody at room temperature for 2 h. The membranes were washed three times with TBST and visualized using enhanced chemiluminescence with a ChemiDoc imaging system (Bio-Rad, California, USA). Three independent replicates were performed.

Surgical denervation of interscapular Brown Adipose Tissue (IBAT)

Surgical IBAT denervation was performed as previously described[65]. The surgery was performed after the chronic alcohol feeding experiments. Each mouse was anesthetized with isoflurane. The mice were shaved and secured on a surgical table. Following a standard skin disinfection procedure with ethanol and iodine swabs, a lateral incision was made to expose the interscapular fat pads. All five branches of the intercostal sympathetic nerves on both sides were connected to the right and left BAT fat pads, which were identified, carefully isolated.

Statistics and reproducibility

Data from each group were represented as the mean ± standard deviation (SD) and examined using GraphPad Prism 9.3 software. Multi-group comparisons were conducted using a one-way or two-way ANOVA. For normally distributed data, statistical comparisons were performed using an unpaired two-tailed Student's *t*-test for two group comparisons. A threshold value of $p < 0.05$ was considered to be statistically significant.

Reporting summary

Further information on research design is available in the Nature Portfolio Reporting Summary linked to this article.

Data availability

The source data underlying the figures can be found in Supplementary Data. The original Western blot images are included in the Supplementary Fig. 9. RNAseq data were deposited into NCBI under accession number PRJNA1071885 and are available at the following URL: https://www.ncbi.nlm.nih.gov/bioproject/PRJNA1071885/. Metabolism data were uploaded into Metabolight under accession number MTBLS10929 and are available at the following URL: https://www.ebi.ac.uk/metabolights/editor/MTBLS10929/descriptors. The used plasmid has been deposited in Addgene with the ID number # 228754.

Received: 16 January 2024; Accepted: 7 November 2024;
Published online: 21 November 2024

References

1. Seitz, H. K. et al. Alcoholic liver disease. *Nat. Rev. Dis. Prim.* **4**, 16 (2018).
2. Singal, A. K. & Shah, V. H. Current trials and novel therapeutic targets for alcoholic hepatitis. *J. Hepatol.* **70**, 305–313 (2019).
3. Thursz, M. R. et al. Prednisolone or pentoxifylline for alcoholic hepatitis. *N. Engl. J. Med* **372**, 1619–1628 (2015).
4. You, M. & Arteel, G. E. Effect of ethanol on lipid metabolism. *J. Hepatol.* **70**, 237–248 (2019).
5. Ashour, M. L. & Wink, M. Genus Bupleurum: a review of its phytochemistry, pharmacology and modes of action. *J. Pharm. Pharm.* **63**, 305–321 (2011).
6. Liang, Z. et al. Cell type-specific qualitative and quantitative analysis of saikosaponins in three Bupleurum species using laser microdissection and liquid chromatography-quadrupole/time of flight-mass spectrometry. *J. Pharm. Biomed. Anal.* **97**, 157–165 (2014).
7. Wang, X. et al. Saikosaponin A of Bupleurum chinense (Chaihu) elevates bone morphogenetic protein 4 (BMP-4) during hepatic stellate cell activation. *Phytomedicine* **20**, 1330–1335 (2013).
8. Bak, S. B. et al. Integrative approach to uncover antioxidant properties of Bupleuri Radix and its active compounds: multiscale interactome-level analysis with experimental validation. *Free Radic. Biol. Med* **199**, 141–153 (2023).
9. Lu, C. N. et al. Saikosaponin a and its epimer saikosaponin d exhibit anti-inflammatory activity by suppressing activation of NF-κB signaling pathway. *Int. Immunopharmacol.* **14**, 121–126 (2012).
10. Fu, Y. et al. Saikosaponin a inhibits lipopolysaccharide-oxidative stress and inflammation in human umbilical vein endothelial cells via preventing TLR4 translocation into lipid rafts. *Free Radic. Biol. Med.* **89**, 777–785 (2015).
11. Sun, Y. et al. Saikosaponin a inhibits the proliferation and activation of T cells through cell cycle arrest and induction of apoptosis. *Int. Immunopharmacol.* **9**, 978–983 (2009).

12. Yuan, B. et al. A systematic review of the active saikosaponins and extracts isolated from Radix Bupleuri and their applications. *Pharm. Biol.* **55**, 620–635 (2017).
13. Shimizu, K. et al. Structural transformation of saikosaponins by gastric juice and intestinal flora. *J. Pharmacobiodyn.* **8**, 718–725 (1985).
14. Fujiwara, K. & Ogihara, Y. Pharmacological effects of oral saikosaponin a may differ depending on conditions of the gastrointestinal tract. *Life Sci.* **39**, 297–301 (1986).
15. Kida, H. et al. Enzymes responsible for the metabolism of saikosaponins from Eubacterium sp. A-44, a human intestinal anaerobe. *Biol. Pharm. Bull.* **20**, 1274–1278 (1997).
16. Wu, Q. J. et al. The sirtuin family in health and disease. *Signal Transduct. Target Ther.* **7**, 402 (2022).
17. Li, Y. et al. Hepatic overexpression of SIRT1 in mice attenuates endoplasmic reticulum stress and insulin resistance in the liver. *FASEB J.* **25**, 1664–1679 (2011).
18. Yang, X. et al. The role and mechanism of SIRT1 in resveratrol-regulated osteoblast autophagy in osteoporosis rats. *Sci. Rep.* **9**, 18424 (2019).
19. Ajmo, J. M. et al. Resveratrol alleviates alcoholic fatty liver in mice. *Am. J. Physiol. Gastrointest. Liver Physiol.* **295**, G833–G842 (2008).
20. You, M. et al. Sirtuin 1 signaling and alcoholic fatty liver disease. *Hepatobiliary Surg. Nutr.* **4**, 88–100 (2015).
21. Purushotham, A. et al. Hepatocyte-specific deletion of SIRT1 alters fatty acid metabolism and results in hepatic steatosis and inflammation. *Cell Metab.* **9**, 327–338 (2009).
22. Bertola, A. et al. Mouse model of chronic and binge ethanol feeding (the NIAAA model). *Nat. Protoc.* **8**, 627–637 (2013).
23. Bertola, A. et al. Chronic plus binge ethanol feeding synergistically induces neutrophil infiltration and liver injury in mice: a critical role for E-selectin. *Hepatology* **58**, 1814–1823 (2013).
24. Zhang, D. et al. The hepatic BMAL1/AKT/lipogenesis axis protects against alcoholic liver disease in mice via promoting the PPARα pathway. *Hepatology* **68**, 883–896 (2018).
25. Montagner, A. et al. Liver PPARα is crucial for whole-body fatty acid homeostasis and is protective against NAFLD. *Gut* **65**, 1202–1214 (2016).
26. Han, J. & Wang, Y. mTORC1 signaling in hepatic lipid metabolism. *Protein Cell* **9**, 145–151 (2018).
27. Chen, H. et al. DEP domain-containing mTOR-interacting protein suppresses lipogenesis and ameliorates hepatic steatosis and acute-on-chronic liver injury in alcoholic liver disease. *Hepatology* **68**, 496–514 (2018).
28. Zhou, Z. et al. Ethanol-induced apoptosis in mouse liver: Fas- and cytochrome c-mediated caspase-3 activation pathway. *Am. J. Pathol.* **159**, 329–338 (2001).
29. Shen, S. et al. SIRT1/SREBPs-mediated regulation of lipid metabolism. *Pharmacol. Res.* **199**, 1007–1037 (2024).
30. Tanno, M. et al. Nucleocytoplasmic shuttling of the NAD+-dependent histone deacetylase SIRT1. *J. Biol. Chem.* **282**, 6823–6832 (2007).
31. Liang, X. et al. Role of SIRT1-FoxO1 signaling in dietary saturated fat-dependent upregulation of liver adiponectin receptor 2 in ethanol-administered mice. *Antioxid. Redox Signal* **15**, 425–435 (2011).
32. Lieber, C. S. et al. Effect of chronic alcohol consumption on hepatic SIRT1 and PGC-1alpha in rats. *Biochem. Biophys. Res. Commun.* **370**, 44–48 (2008).
33. You, M. et al. Involvement of mammalian sirtuin 1 in the action of ethanol in the liver. *Am. J. Physiol. Gastrointest. Liver Physiol.* **294**, G892–G898 (2008).
34. Dai, X. et al. Solubilization of saikosaponin A by ginsenoside Ro biosurfactant in aqueous solution: mesoscopic simulation. *J. Colloid Interface Sci.* **384**, 73–80 (2012).
35. Yang, M. L. et al. Pharmacokinetics of eight constituents in rat plasma after oral administration of modified Xiaochaihu granules for gastric ulcer based on UPLC-MS/MS. *Zhongguo Zhong Yao Za Zhi* **43**, 3748–3755 (2018).
36. Ren, R. et al. Emerging roles of SIRT1 in alcoholic liver disease. *Int. J. Biol. Sci.* **16**, 3174–3183 (2020).
37. Shibata, M. et al. Some pharmacological effects of crude saikosides, saikogenin A, and syrupy residue. *Yakugaku Zasshi* **93**, 1660–1667 (1973).
38. Cheng, J. T. & Tsai, C. L. Anti-inflammatory effect of saikogenin A. *Biochem. Pharm.* **35**, 2483–2487 (1986).
39. Mackowiak, B. et al. Alcohol-associated liver disease. *J. Clin. Invest.* **134**, e176345 (2024).
40. Singal, A. K. et al. ACG clinical guideline: alcoholic liver disease. *Am. J. Gastroenterol.* **113**, 175–194 (2018).
41. Louvet, A. & Mathurin, P. Alcoholic liver disease: mechanisms of injury and targeted treatment. *Nat. Rev. Gastroenterol. Hepatol.* **12**, 231–242 (2015).
42. Jeon, S. & Carr, R. Alcohol effects on hepatic lipid metabolism. *J. Lipid Res.* **61**, 470–479 (2020).
43. Day, C. P. & James, O. F. Hepatic steatosis: innocent bystander or guilty party. *Hepatology* **27**, 1463–1466 (1998).
44. Zhong, W. et al. Chronic alcohol exposure stimulates adipose tissue lipolysis in mice: role of reverse triglyceride transport in the pathogenesis of alcoholic steatosis. *Am. J. Pathol.* **180**, 998–1007 (2012).
45. Zhu, Y. et al. Saikosaponin A ameliorates lipopolysaccharide and d-galactosamine-induced liver injury via activating LXRα. *Int. Immunopharmacol.* **72**, 131–137 (2019).
46. Li, X. et al. Integrative lipidomic and transcriptomic study unravels the therapeutic effects of saikosaponins A and D on non-alcoholic fatty liver disease. *Acta Pharm. Sin. B* **11**, 3527–3541 (2021).
47. Wu, S. J. et al. Curcumin and saikosaponin A inhibit chemical-induced liver inflammation and fibrosis in rats. *Am. J. Chin. Med.* **38**, 99–111 (2010).
48. Tu, Y. et al. Natural compounds in the chemoprevention of alcoholic liver disease. *Phytother. Res.* **33**, 2192–2212 (2019).
49. Majeed, Y. et al. SIRT1 promotes lipid metabolism and mitochondrial biogenesis in adipocytes and coordinates adipogenesis by targeting key enzymatic pathways. *Sci. Rep.* **11**, 8177 (2021).
50. Singh, V. & Ubaid, S. Role of silent information regulator 1 (SIRT1) in regulating oxidative stress and inflammation. *Inflammation* **43**, 1589–1598 (2020).
51. Farzaei, M. H. et al. Curcumin in liver diseases: a systematic review of the cellular mechanisms of oxidative stress and clinical perspective. *Nutrients* **10**, 855 (2018).
52. Li, B. Y. et al. Protective effects of tea extracts against alcoholic fatty liver disease in mice via modulating cytochrome P450 2E1 expression and ameliorating oxidative damage. *Food Sci. Nutr.* **9**, 5626–5640 (2021).
53. Zhang, P. et al. Berberine protects liver from ethanol-induced oxidative stress and steatosis in mice. *Food Chem. Toxicol.* **74**, 225–232 (2014).
54. Zhou, Z. S. et al. Fisetin ameliorates alcohol-induced liver injury through regulating SIRT1 and SphK1 pathway. *Am. J. Chin. Med.* **50**, 2171–2184 (2022).
55. Yin, F. et al. Hepatic NCoR1 deletion exacerbates alcohol-induced liver injury in mice by promoting CCL2-mediated monocyte-derived macrophage infiltration. *Acta Pharm. Sin.* **43**, 2351–2361 (2022).
56. Chao, X. et al. Impaired TFEB-mediated lysosome biogenesis and autophagy promote chronic ethanol-induced liver injury and steatosis in mice. *Gastroenterology* **155**, 865–879.e12 (2018).
57. Evans, C. R. et al. Untargeted metabolomics differentiates l-carnitine treated septic shock 1-year survivors and nonsurvivors. *J. Proteome Res.* **18**, 2004–2011 (2019).

58. Wang, S. et al. Nicotinamide riboside attenuates alcohol-induced liver injuries via activation of SIRT1/PGC-1α/mitochondrial biosynthesis pathway. *Redox Biol.* **17**, 89–98 (2018).
59. Zhao, Y. et al. Melatonin prevents ethanol-induced liver injury by mitigating ferroptosis via targeting brain and muscle ARNT-like 1 in mice liver and HepG2 cells. *J. Agric. Food Chem.* **70**, 12953–12967 (2022).
60. Kudo, Y. et al. PKCλ/ι loss induces autophagy, oxidative phosphorylation, and NRF2 to promote liver cancer progression. *Cancer Cell* **38**, 247–262.e11 (2020).
61. Guo, Y. et al. Baohuoside-1 targeting mTOR induces apoptosis to inhibit hepatocellular carcinoma proliferation, invasion, and migration. *Biomed. Pharmacother.* **128**, 110366 (2020).
62. Babuta, M. et al. Dysregulated autophagy and lysosome function are linked to exosome production by micro-RNA 155 in alcoholic liver disease. *Hepatology* **70**, 2123–2141 (2019).
63. Dai, H. et al. Crystallographic structure of a small molecule SIRT1 activator-enzyme complex. *Nat. Commun.* **6**, 7645 (2015).
64. Pan, B. et al. Chinese herbal compounds against SARS-CoV-2: puerarin and quercetin impair the binding of viral S-protein to ACE2 receptor. *Comput. Struct. Biotechnol. J.* **18**, 3518–3527 (2020).
65. Munoz, M. D. et al. Activation of brown adipose tissue by a low-protein diet ameliorates hyperglycemia in a diabetic lipodystrophy mouse model. *Sci. Rep.* **13**, 11808 (2023).

Acknowledgements

This research was financially supported by the National Natural Science Foundation of China (No. 82371596, 82073232, 81700769, and 81641028), the Hubei Province Science and Technology Department Innovation Group Project (2023AFA023), the Advantages Discipline Group(Medicine) Project in Higher Education of Hubei Province (2024XKQY51), the Hubei Province Science and Technology Plan Project (2023BCB137), the Hubei Province Science and Technology Department of Natural Science Foundation (2024AFB787, 2024AFD324), Hubei Provincial Natural Science Foundation Innovation and Development Joint Fund Project (2024AFD324), the Project of Creative Research Groups of Hubei Province (2021CFB247), The open Project of Hubei Key Laboratory of Wudang Local Chinese Medicine Research (Hubei University of Medicine) (Grant No.WDCM2023018).

Author contributions

Mingzhu Jiang, Yufeng Wang, Xingrong Guo, Tongfei Li, and Shiming Du, contributed to the conception and design of the study. Mingzhu Jiang, Jingxian Wang, and Xiang Xu contributed to acquisition and analysis of data. Mingzhu Jiang, Ying Feng, Xingrong Guo, Yufeng Wang, Shinan Ma, and Zegan Liu contributed to drafting the manuscript and figures.

Competing interests

The authors declare no competing interests.

Additional information

Supplementary information The online version contains supplementary material available at https://doi.org/10.1038/s42003-024-07234-x.

Correspondence and requests for materials should be addressed to Yufeng Wang, Xingrong Guo or Shiming Du.

Peer review information *Communications Biology* thanks Kung-Chia Young and Rakesh Arya for their contribution to the peer review of this work. Primary Handling Editors: Christina Karlsson Rosenthal. A peer review file is available.